Journal of Environmental Protection, 2016, 7, 1605-1617
http://www.scirp.org/journal/jep
ISSN Online: 2152-2219
ISSN Print: 2152-2197

Morphology-Controlled Synthesis of $Zn_xCd_{1-x}S$ Solid Solutions: An Efficient Solar Light Active Photocatalyst for the Degradation of 2,4,6-Trichlorophenol

Rengaraj Selvaraj[1,2*], Kezhen Qi[3], Sathish Babu Soundra Pandian[4], Mohammed A. Meetani[5], Bushra Al Wahaibi[1], Haider Al Lawati[1], Salma M. Z. Al Kindy[1], Younghun Kim[6], Mika Sillanpää[2]

[1]Department of Chemistry, College of Science, Sultan Qaboos University, Muscat, Sultanate of Oman
[2]Laboratory of Green Chemistry, LUT Savo Sustainable Technology, Lappeenranta University of Technology, Mikkeli, Finland
[3]Institute of Catalysis for Energy and Environment, College of Chemistry and Chemical Engineering, Shenyang Normal University, Shenyang, China
[4]CAARU, College of Science, Sultan Qaboos University, Muscat, Sultanate of Oman
[5]Department of Chemistry, United Arab Emirates University, Al Ain, UAE
[6]Department of Chemical Engineering, Kwangwoon University, Seoul, South Korea
Email: *srengaraj1971@yahoo.com

How to cite this paper: Selvaraj, R., Qi, K.Z., Pandian, S.B.S., Meetani, M.A., Al Wahaibi, B., Al Lawati, H., Al Kindy, S.M.Z., Kim, Y. and Sillanpää, M. (2016) Morphology-Controlled Synthesis of $Zn_xCd_{1-x}S$ Solid Solutions: An Efficient Solar Light Active Photocatalyst for the Degradation of 2,4,6-Trichlorophenol. *Journal of Environmental Protection*, **7**, 1605-1617.
http://dx.doi.org/10.4236/jep.2016.711132

Received: September 28, 2016
Accepted: October 25, 2016
Published: October 28, 2016

Abstract

$Zn_xCd_{1-x}S$ solid solutions with controlled morphology have been successfully synthesized by a facile solution-phase method. The prepared samples were characterized by X-ray powder diffraction (XRD), UV-vis diffuse reflectance spectra, X-ray photoelectron spectroscopy (XPS), scanning electron microscopy (SEM) and transmission electron microscopy (TEM). The photocatalytic activity of $Zn_xCd_{1-x}S$ was evaluated in the 2,4,6-trichlorophenol (TCP) degradation and mineralization in aqueous solution under direct solar light illumination. The experiment demonstrated that TCP was effectively degraded by more than 95% with 120 min. The results show that ZnS with Cd doping ($Zn_xCd_{1-x}S$) exhibits the much stronger visible light adsorption than that of pure ZnS, the light adsorption increasing as the Cd^{2+} doping amount. These results indicate that Cd doping into a ZnS crystal lattice can result in the shift of the valence band of ZnS to a positive direction. It may lead to its higher oxidative ability than pure ZnS, which is important for organic pollutant degradation under solar light irradiation. Furthermore, the photocatalytic activity studies reveal that the prepared $Zn_xCd_{1-x}S$ nanostructures exhibit an excellent photocatalytic performance, degrading rapidly the aqueous 2,4,6-trichlorophenol solution under solar light irradiation. These results suggest that $Zn_xCd_{1-x}S$ nanostructure will be a promising candidate of photocatalyst working in solar light range.

Keywords

Photocatalyst, Nanostructures, Solution Phase, 2,4,6-Trichlorophenol, Solar Light, Photocatalytic Activity

1. Introduction

Among the water contaminants, chlorophenols are the most hazardous class of water pollutants [1]. Chlorophenols (CPs) are used in many industries such as paint, pharmaceutical, pesticide, solvent, wood, paper, and pulp industries [2]. However, these CPs are very harmful to humans because they are toxic, mutagenic and carcinogenic. They affect the nervous system and cause respiratory problems [3]. They must be decomposed before discharging to the rivers or lakes. Under this background, it is of importance to find an easy and effective method to completely remove these chlorinated organic pollutants [4].

During recent decades, semiconductor based photocatalysis has been extensively studied and has become one of the most promising methods in environmental protection procedures such as air and water purification and hazardous waste remediation [5]. TiO_2 nanomaterials have often been used as photocatalysts because of their efficiency, stability, non-toxicity, and low cost [6]. However, it has some drawbacks such as the relatively high value of the band gap energy (~3.2 eV), which limits its absorption to the UV spectral region, and the high recombination rate of photo-induced electrons and holes, which decreases its photocatalytic activity [7]. Therefore, many efforts have focused on investigating high-efficiency visible-light photocatalysts because of their potential for various applications, including environmental pollution control and solar energy utilization.

Metal sulfides have been intensively studied as active photocatalysts because of their high light harvesting for promoting charge separation [8]-[12]. For example, CdS shows a high photocatalytic activity in water splitting for hydrogen production [13]. However, there remain some drawbacks including fast recombination of photogenerated electron-hole pairs and suffer from severe photocorrosion, both of which prohibit the wide application of CdS. To solve these problems, forming CdS/ZnS heterojunction structure is an effective method, because the same coordination mode between CdS and ZnS will promote interfacial charge transfer and inhibit the photo-corrosion of CdS via dispersing ZnS on the surface as well [14]. The key point of this CdS/ZnS heterojunction is to achieve a strong join between CdS and ZnS intersurface and the uniform distribution of each kind of atoms inside bulk material. Moreover, the electronic structure of the $Zn_xCd_{1-x}S$ solid solution can be easily controlled by tuning the molar ratio of Zn^{2+} and Cd^{2+} [15]. Therefore, the synthesis of $Zn_{1-x}Cd_xS$ solid solutions is of immense interest and increasing technological importance for future applications.

The controlled synthesis of inorganic nanomaterials with desired morphology has received considerable attention due to the physical and chemical properties of sold na-

nomaterials specially depend on their phase, size, shape, and organization [16]-[25]. Over the past few years, many methods have been developed to synthesize $Zn_xCd_{1-x}S$ solid solutions with controlled morphology, such as solid state reactions [26], solution-phase process [27], cation exchange reactions [28], and microwave synthesis [29]. However, it is still a big challenge to find an easy way to prepare $Zn_xCd_{1-x}S$ solid solutions with controlled morphology. Also unfortunately, there has been no report available for the degradation of 2,4,6-trichlorophenol using $Zn_xCd_{1-x}S$ solid solutions. In this paper, we report for the first time on the photocatalytic degradation of 2,4,6-trichlorophenol (TCP). The result shows that, with the increase of Cd molar fraction, the character of UV-visible absorption of $Zn_xCd_{1-x}S$ crystal gradually evolves from ZnS to CdS, and this $Zn_xCd_{1-x}S$ sample under solar irradiation demonstrates a considerable photocatalytic degradation of aqueous 2,4,6–trichlorophenol (TCP).

2. Experimental

2.1. Synthesis of $Zn_xCd_{1-x}S$ Samples

The $Zn_xCd_{1-x}S$ solid solutions with different Cd molar ratios were prepared with $Cd(NO_3)_2{\cdot}4H_2O$, $Zn(NO_3)_2{\cdot}6H_2O$ and thioacetamide. The $Zn_xCd_{1-x}S$ solid solutions were prepared according to the previous reported methods [26] [27]. All chemicals were purchased as guaranteed regents and used without further purification. The stock solution was prepared by dissolving amount of $Cd(NO_3)_2{\cdot}4H_2O$, $Zn(NO_3)_2{\cdot}6H_2O$ and thioacetamide in a 250 mL round bottom flask and by filling with 100 mL of distilled water. Afterwards, the stock solution was heated to reflux at 105˚C. After the mixture was refluxed for 45 min, a precipitate was obtained, which was filtered then washed with absolute ethanol and distilled water several times. After being dried in oven at 60˚C for 24 hours, the products were collected for characterization.

2.2. Characterization

The crystalline properties of Cd doping ZnS nanocrystals were studied by X-ray diffraction (XRD) using a Bruker (D5005) X-ray diffractometer equipped with graphite monochromatized CuK_α radiation (λ = 1.54056 Å). The crystal morphology was examined by field emission scanning electron microscopy (FESEM) and transmission electron microscopy (TEM). The FESEM images were obtained from Hitachi S-4800, which is equipped with an energy dispersive X-ray spectrometer (EDX). The lattice spacing of the products was also taken by high resolution TEM (HRTEM) (JEOL JEM-3010). The chemical states and relative compositions of the samples were studied by X-ray photoelectron spectroscopy (XPS) (ThermoVG, U.K) with a monochromatized Al Kα irradiation (1.4867 eV) and a pass energy of 20 eV. All XPS spectra were obtained with an energy step of 0.1 eV and a dwell time of 50 ms. An Avantage Thermo VG software was used to analyze the XPS data. The absorption spectra of the as-prepared samples were recorded using a UV-Vis diffuse reflectance spectroscopy (DRS) (Jasco V670) in the wavelength range of 200 - 1000 nm, with $BaSO_4$ as a reference.

2.3. Photocatalytic Degradation of 2,4,6-Trichlorophenol

Photocatalytic reactions were performed in a cylindrical borosilicate glass reactor vessel with the volume of 250 mL, with a simulated solar light irradiation for the degradation of 2,4,6-trichlorophenol and a recycling water jacket to keep cooling. The photocatalytic tests were performed with 100 mg of catalyst suspended in 2,4,6-trichlorophenol aqueous solution (250 mL, 5mg/L). The concentration of 2,4,6-trichlorophenol left in the centrifuged aqueous solution was determined by LC/MS spectrophotometer (Model: Agilent Technologies–6460 Triple quad LC/MS), in which Water Symmetry C-8 column (3.5 micro Mt-2.1 × 150–Part No.: WAT106011) was used and mobile phase of methanol/water (95:5 v/v) with 5 mmol ammonium acetate was employed at a flow rate of 0.5 mL/min.

3. Results and Discussion

3.1. Phase Structures

Figure 1 shows the XRD patterns of the as prepared $Zn_xCd_{1-x}S$ (x = 0, 0.2, 0.5, 0.8 and 1) samples. These samples show the similar pattern, and all the diffraction peaks can be well indexed to the cubic ZnS (JCPDS Card No. 75 - 1547). When a small amount of Cd was doped into the ZnS crystal, (for example, $Zn_{0.8}Cd_{0.2}S$), the diffraction peaks of ZnS exhibited an obvious shift toward the lower angle. This implies that Cd^{2+} incorporates into the ZnS crystal lattice and increases the fringe lattice distance of the ZnS crystal due to the larger radius of Cd^{2+} (0.97 Å) than that of the Zn^{2+} ion (0.74 Å) [30]. With

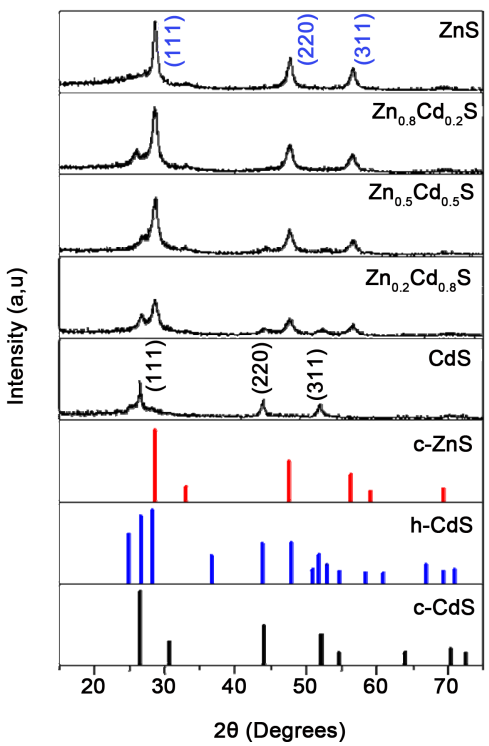

Figure 1. XRD patterns of morphology-controlled $Zn_xCd_{1-x}S$ samples.

increasing Cd^{2+} content in the $Zn_xCd_{1-x}S$ solid solution, the XRD peak positions continuously shift to low angle side, and the crystal phase of the $Zn_xCd_{1-x}S$ solid solution gradually changes from the cubic to hexagonal phase and finally becomes the hexagonal wurtzite CdS phase for the CdS sample (JCPDS Card No. 42-1411). This implies that the Cd^{2+} in the ZnS crystal influence the positions of Zn^{2+} and consequently change the lattice structure of ZnS during the formation of the $Zn_xCd_{1-x}S$ solid solutions.

3.2. UV-Visible Diffuse Reflection Spectra

The optical properties of $Zn_xCd_{1-x}S$ nanostrucures are examined by using UV-vis DRS spectrum, as shown in **Figure 2(a)**. With increasing the molar ratio of Cd^{2+}/Zn^{2+}, the absorption edge of $Zn_xCd_{1-x}S$ shows an obvious red shift. This red shift indicates that the electronic structure of $Zn_xCd_{1-x}S$ nanostrucures can be easily turned by the changing the Zn^{2+}/Cd^{2+} molar ratios in precursors. The samples are changed from white to yellow.

The optical absorption follows the equation $\acute{a}hv = A(h\acute{i}-E_g)^{n/2}$, where á, í, E_g and A are the absorption coefficient, the light frequency, the band gap and a constant, respectively. Among them, n determines the characteristics of the transition in a semiconductor [31]. The band gaps are measured to be about 2.22, 2.14 and 2.05 eV for x = 0.2, 0.5 and 0.8 $Zn_xCd_{1-x}S$, respectively (**Figure 2(b)**), which incorporated Cd^{2+} into the ZnS crystal lattice and induced the band gap narrowing.

3.3. XPS Study

In order to study the compositions on $Cd_{0.5}Zn_{0.5}S$ surface, XPS measurements are carried out. **Figure 3(a)** shows the wide spectrum of the $Zn_{0.5}Cd_{0.5}S$ sample, which confirms the presence of Zn, Cd, S, O and C in the sample. The observed C and O peaks is due to the carbon supporting film used for measurement and the adsorbed oxygen molecules on the sample surface, respectively.

Figures 3(b)-(d) shows that the high-resolution XPS spectra of $Zn_{0.5}Cd_{0.5}S$. The peaks at 404.9 (Cd $3d_{5/2}$), 411.7 (Cd $3d_{3/2}$), 1045.5 (Zn $2p_{1/2}$), 1022.3 (Zn $2p_{3/2}$), 163.0 (S $2p_{1/2}$) and 162.0 (S $2p_{3/2}$) were attributed to the $Cd_{0.5}Zn_{0.5}S$ surface condition, which

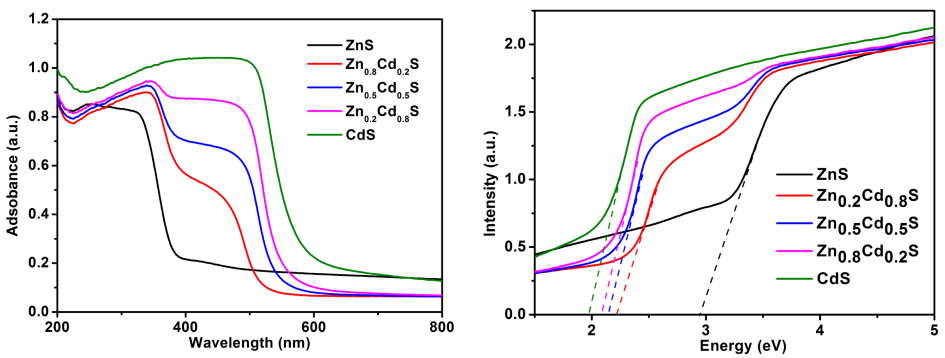

(a) (b)

Figure 2. (a) UV-vis DRS spectra and (b) plot of transformed the energy of the light absorbed for the $Zn_xCd_{1-x}S$ samples.

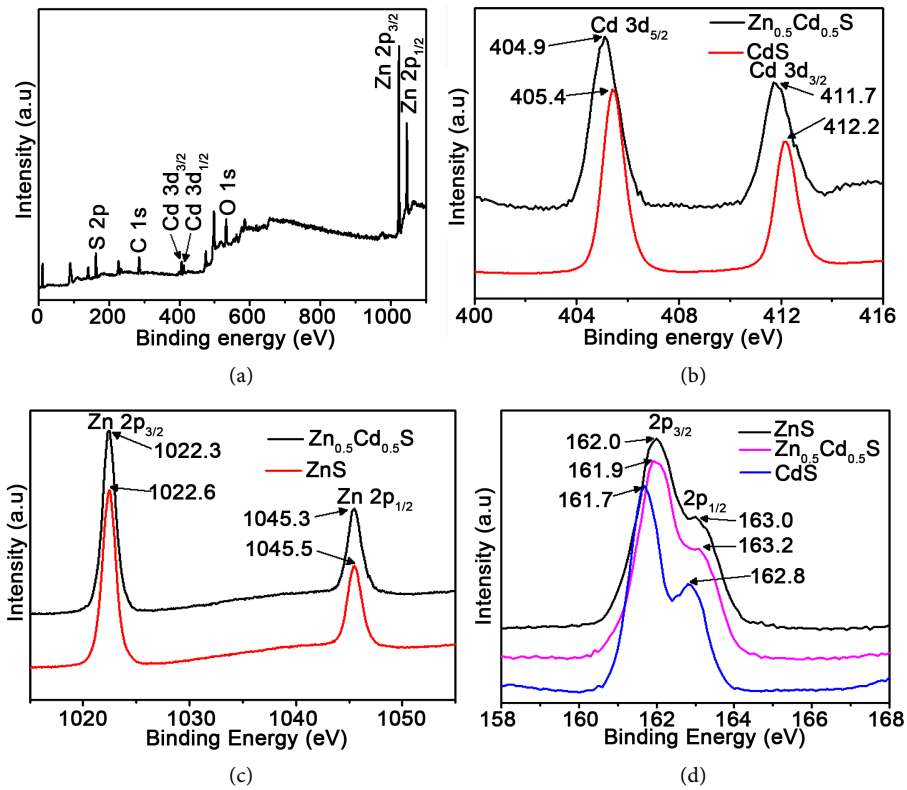

Figure 3. XPS survey spectrum of (a) $Cd_{0.5}Zn_{0.5}S$ and high-resolution XPS spectra of (b) Cd 3d; (c) Zn 2p and (d) S 2p for the $Cd_{0.5}Zn_{0.5}S$ sample.

agree well with the results reported by Yang *et al.* [32] Compare to ZnS, Zn peak of the $Cd_{0.5}Zn_{0.5}S$ show a shift toward low degree (**Figure 3(b)**). Compare to CdS, Cd peak of the $Cd_{0.5}Zn_{0.5}S$ show a shift toward low degree (**Figure 3(c)**). Compare to ZnS and CdS, S peak of the $Cd_{0.5}Zn_{0.5}S$ is in the middle (**Figure 3(d)**).

3.4. SEM Morphology Analysis

SEM measurement was used to investigate the influence of Cd^{2+} doping on the morphology of ZnS nanocrystals, as shown in **Figure 4**. The ZnS sample is composed of the sphere-like nanostructures about 2.5 - 3.0 μm in diameter, the sphere is composed of small nanoparticles (**Figure 4(a)**). When molar ratio of Zn^{2+} to Cd^{2+} is 0.8:0.2, the product is composed of the sphere-like nanostructures illustrated in **Figure 4(b)**, the diameter is about 250 - 300 nm the surface is a little rough. When the molar ratio is 0.5:0.5, the diameters of the spheres are 200 - 300 nm and 80-100 nm, the size is not uniform (**Figure 4(c)**). When the molar ratio is decreased to 0.2:0.8, the diameters of the spheres are in the range of 250 - 270 nm with uniform size (**Figure 4(d)**). The CdS sample is composed of the sphere-like nanostructures about 1.5 - 3.0 μm in diameter, the sphere surface is smooth (**Figure 4(e)**). These SEM results indicate that the general morphology of these $Zn_xCd_{1-x}S$ solid solutions is almost the same, small particles assemble for big particles. However, it is apparent that the diameter of the individual $Zn_xCd_{1-x}S$ spherical particle can be controlled by turning the ratio of Zn^{2+} to Cd^{2+}.

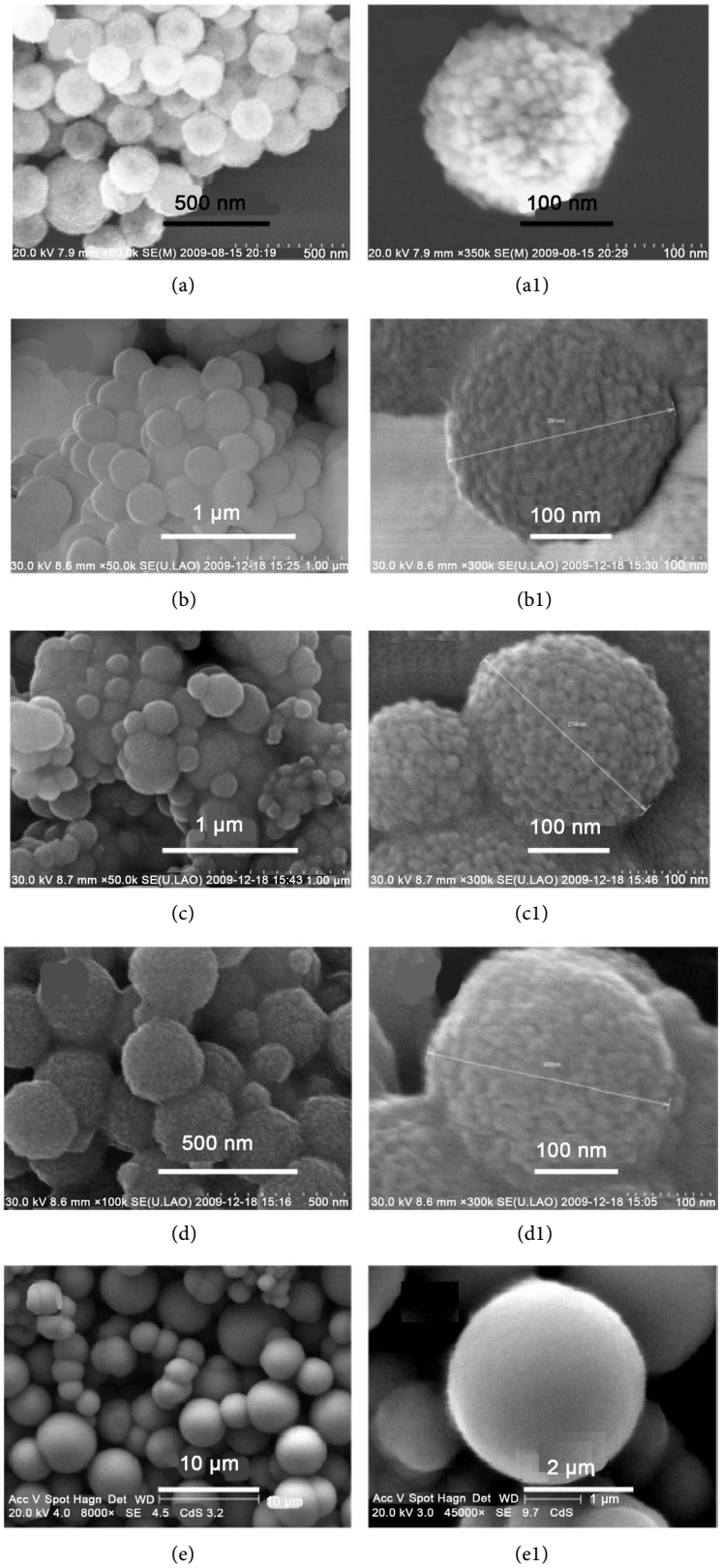

Figure 4. SEM images of the as-prepared $Zn_xCd_{1-x}S$ samples: (a, a1) x = 1, (b, b1) x = 0.8; (c, c1) x = 0.5; (d, d1) x = 0.2; (e, e1) x = 0.

3.5. TEM Test for Samples

The morphologies of as prepared ZnS, $Zn_xCd_{1-x}S$ and CdS samples are investigated using TEM and HRTEM analysis, respectively (**Figure 5**). From the TEM images of as synthesized ZnS samples, it can be seen that the product was present in a large scare spherical with the diameter in 100 - 120 nm (**Figure 5(a)**). There is also spherical particle shape but no uniform size for the as-synthesized $Cd_xZn_{1-x}S$ sample (choose $Zn_{0.5}Cd_{0.5}S$ as an example). Some size is around 50 nm some size is around 300 nm (**Figure 5(b)**). For the CdS sample, make up some irregular nanoparticles with the size of 20-40 nm (**Figure 5(c)**). The diameter of this nanoparticle is consistent with the result from the XRD data according to the calculation of Scherrer Formula. The components of the products were further confirmed by EDX, which indicates that the ratio of Zn, Cd and S is 0.5:0.5:1 for $Zn_{0.5}Cd_{0.5}S$ (**Figures 5(a1)-(c1)**), which is consistent with the XPS result above (**Figure 3**).

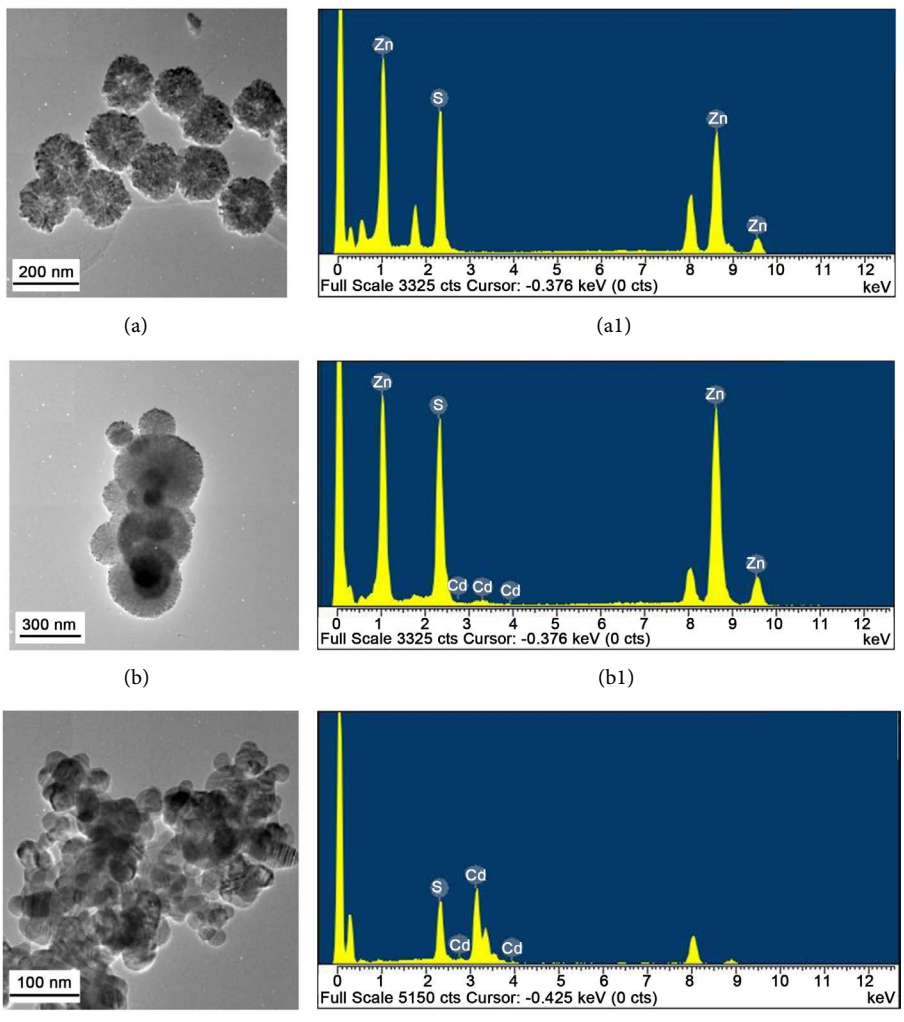

Figure 5. TEM and HRTEM images of as-synthesized (a) ZnS; (b) $Cd_{0.5}Zn_{0.5}S$ and (c) CdS, and the corresponding EDX spectrum.

3.6. Photocatalytic Activity Test

In order to evaluate the photocatalytic activity of $Zn_xCd_{1-x}S$ samples, photodegradation of TCP was carried out in aqueous suspension using pure ZnS and $Zn_xCd_{1-x}S$ catalysts with a different Cd content between 0.2 and 0.8 mole ratio, and the experimental results are shown in Figure 6. Figure 7 represents the time-dependent LC/MS peak intensity of the TCP solution during photo degradation in the presence of CdS microspheres. The peak intensity at around 0.9 min decreased gradually with irradiation time. The experiment demonstrated that TCP was effectively degraded by more than 95% with 120 min. At the end of the degradation after 240 min, no peak could be detected, implying that complete oxidation of TCP occurred due to the presence of CdS microsphere under solar light irradiation. A bigger doping amount of Cd on ZnS can be detrimental to the TCP photodegradation efficiency.

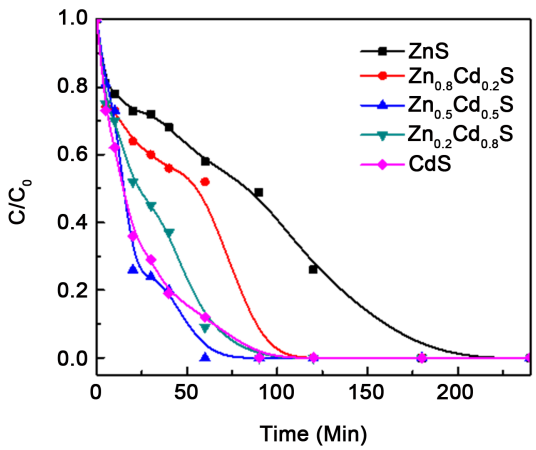

Figure 6. Photocatalytic degradation of 2,4,6-Trichlorophenol under solar light irradiation by $Zn_xCd_{1-x}S$ solid solutions. (Catalyst dosage: 100 mg/250 mL; concentration of 2,4,6-Trichlorophenol: 5 mg/L).

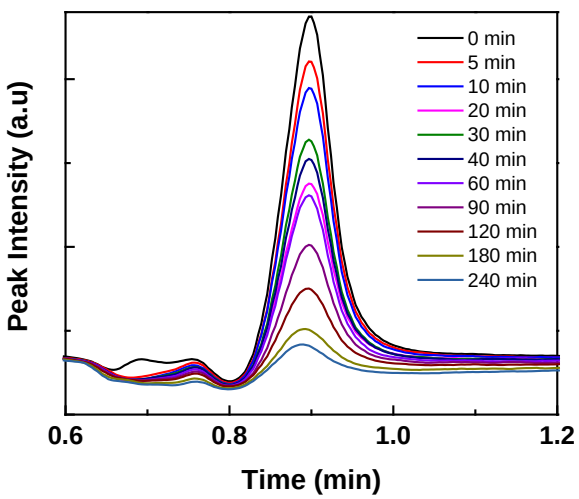

Figure 7. Variation of 2,4,6-trichlorophenol degradation with time by CdS under solar light irradiation.

Figure 6 shows that the photocatalytic activity of $Zn_{0.5}Cd_{0.5}S$ for degradation of TCP is much higher than that of pure ZnS. This result indicates that doping Cd ions promotes the charge pair separation efficiency for ZnS catalysts. The electron activates from the conduction band of ZnS to Cd atoms is thermodynamically due to the Fermi level of ZnS is higher than that of Cd metal [33] [34]. This results in the formation of a Schottky barrier at metal-semiconductor contact region and improves the efficiency of charge separation of ZnS [35] [36]. Contrarily, at the high content of Cd doping, Cd atoms also will act as a recombination center and decrease the photocatalytic activity of ZnS. From this work, the as prepared $Zn_xCd_{1-x}S$ samples demonstrated an excellent performance in photocatalytic degradation of aqueous TCP solution under solar irradiation.

4. Conclusion

In the present study, the feasibility of employing $Zn_xCd_{1-x}S$ solid solutions for the degradation of 2,4,6-trichlorophenol has been demonstrated successfully. $Zn_xCd_{1-x}S$ solid solutions with tunable chemical composition and controlled morphology have been successfully synthesized by a facile solution-phase method without the use of any surfactants. The $Zn_xCd_{1-x}S$ products demonstrate well-dispersed spheres with different diameters. With the increase of Cd molar fractions, the UV-visible absorption of $Zn_xCd_{1-x}S$ crystal gradually evolves from ZnS to CdS, which leads to that the $Zn_xCd_{1-x}S$ sample under solar irradiation demonstrates a considerable photocatalytic degradation of 2,4,6-Trichlorophenol in aqueous solution.

Acknowledgements

The authors (RS and MAM) are grateful to Sultan Qaboos University for providing financial support to carry out this work under SQU-UAEU joint collaborative research grant (CL/SQU-UAEU/16/04).

Declare

The authors declare no competing financial interest.

References

[1] Aslam, M., Soomro, M.T., Ismail, I.M.I., Salah, N., Gondal, M.A. and Hameed, A. (2015) Sunlight Mediated Removal of Chlorophenols over Tungsten Supported ZnO: Electrochemical and Photocatalytic Studies. *Journal of Environmental Chemical Engineering*, **3**, 1901-1911. http://dx.doi.org/10.1016/j.jece.2015.07.004

[2] Abbas, H.A., Jamil, T.S. and Hammad, F.F. (2016) Synthesis, Characterization and Photocatalytic activIty of Nano sized Undoped and Ga Doped $SrTi_{0.7}Fe_{0.3}O_3$ for 2,4,6-Trichlorophenol Photodegradation. *Journal of Environmental Chemical Engineering*, **4**, 2384-2393. http://dx.doi.org/10.1016/j.jece.2016.04.019

[3] Chaliha, S. and Bhattacharya, K.G. (2008) Catalytic Wet Oxidation of 2-Chlorophenol, 2,4-Dichlorophenol and 2,4,6-Trichlorophenol in Water with Mn(II)-MCM41. *Chemical Engineering Journal*, **139**, 575-588. http://dx.doi.org/10.1016/j.cej.2007.09.006

[4] Rengaraj, S. and Li, X.Z. (2006) Enhanced Photocatalytic Activity of TiO_2 by Doping with Ag for Degradation of 2,4,6-Trichlorophenol in Aqueous Suspension. *Journal of Molecular Catalysis A*: *Chemical*, **243**, 60-67. http://dx.doi.org/10.1016/j.molcata.2005.08.010

[5] Carevic, M., Abazovic, N.D., Savic, T., Novakovic, T.B., Mojovic, M.D. and Comor, M.I. (2016) Structural, Optical and Photodegradation Properties of Pure and Fe-Doped Titania Nanoparticles Probed Using Simulated Solar Light. *Ceramics International*, **42**, 1521-1529. http://dx.doi.org/10.1016/j.ceramint.2015.09.100

[6] Tong, Z., Yang, D., Xiao, T., Tian, Y. and Jiang, Z. (2015) Biomimetic Fabrication of g-C_3N_4/TiO_2 Nanosheets with Enhanced Photocatalytic Activity toward Organic Pollutant Degradation. *Chemical Engineering Journal*, **260**, 117-125. http://dx.doi.org/10.1016/j.cej.2014.08.072

[7] Yang, J., Cui, S.H., Qiao, J. and Lian, H.-Z. (2014) The Photocatalytic Dehalogenation of Chlorophenols and Bromophenols by Cobalt Doped Nano TiO_2. *Journal of Molecular Catalysis A*: *Chemical*, **395**, 42-51. http://dx.doi.org/10.1016/j.molcata.2014.08.001

[8] Habisreutinge, S.N., Mende, L.S. and Stolarczyk, J.K. (2013) Photocatalytic Reduction of CO_2 on TiO_2 and Other Semiconductors. *Angewandte Chemie International Edition*, **52**, 7372-7408. http://dx.doi.org/10.1002/anie.201207199

[9] Xiang, Q.J., Yu, J.G. and Jaroniec, M. (2012) Synergetic Effect of MoS_2 and Graphene as Cocatalysts for Enhanced Photocatalytic H_2 Production Activity of TiO_2 Nanoparticles. *Journal of the American Chemical Society*, **134**, 6575-6578. http://dx.doi.org/10.1021/ja302846n

[10] Zhang, J., Liu, S.W., Yu, J.G. and Jaroniec, M. (2011) A Simple Cation Exchange Approach to Bi-Doped ZnS Hollow Spheres with Enhanced UV and Visible-Light Photocatalytic H_2-Production Activity. *Journal of Materials Chemistry*, **21**, 14655-14662. http://dx.doi.org/10.1039/c1jm12596f

[11] Li, Q., Guo, B.D., Yu, J.G., Ran, J.R., Zhang, B.H., Yan, H.J. and Gong, J.R. (2011) Highly Efficient Visible-Light-Driven Photocatalytic Hydrogen Production of CdS-Cluster-Decorated Graphene Nanosheets. *Journal of the American Chemical Society*, **133**, 10878-10884. http://dx.doi.org/10.1021/ja2025454

[12] Zhang, J., Qiao, S.Z., Qi, L. and Yu, J. (2013) Fabrication of NiS Modified CdS Nanorod p-n Junction Photocatalysts with Enhanced Visible-Light Photocatalytic H_2-Production Activity. *Physical Chemistry Chemical Physics*, **15**, 12088-12094. http://dx.doi.org/10.1039/c3cp50734c

[13] Xiang, Q.J. and Yu, J.G. (2013) Graphene-Based Photocatalysts for Hydrogen Generation. *The Journal of Physical Chemistry Letters*, **4**, 753-759. http://dx.doi.org/10.1021/jz302048d

[14] Soltani, N., Saiona, E., Yunus, W.M.M., Erfani, M., Navasery, M., Bahmanrokh, G. and Rezaee, K. (2014) Enhancement of Visible Light Photocatalytic Activity of ZnS and CdS Nanoparticles Based on Organic and Inorganic Coating. *Applied Surface Science*, **290**, 440-447. http://dx.doi.org/10.1016/j.apsusc.2013.11.104

[15] Wu, J.C., Zheng, J., Zacherl, C.L., Wu, P., Liu, Z.K. and Xu, R. (2011) Hybrid Functionals Physical Chemistry Chemical PhysicsStudy of Band Bowing, Band Edges and Electronic Structures of $Cd_{1-x}Zn_xS$ Solid Solution. *The Journal of Physical Chemistry C*, **115**, 19741-19748. http://dx.doi.org/10.1021/jp204799q

[16] Zhang, Q., Du, Q., Hua, M., Jiao, T., Gao, F. and Pan, B. (2013) Sorption Enhancement of Lead Ions from Water by Surface Charged Polystyrene-Supported Nano-Zirconium Oxide Composites. *Environmental Science & Technology*, **47**, 6536-6544. http://dx.doi.org/10.1021/es400919t

[17] Li, X., Yu, J. and Jaroniec, M. (2016) Hierarchical Photocatalysts. *Chemical Society Reviews*, **45**, 2603-2636. http://dx.doi.org/10.1039/C5CS00838G

[18] Qi, K.Z., Yang, J.Q., Fu, J.Q., Wang, G.C., Zhu, L.J., Liu, G. and Zheng, W.J. (2013) Morphology-Controllable ZnO Rings: Ionic Liquid-Assisted Hydrothermal Synthesis, Growth Mechanism and Photoluminescence Properties. *CrystEngComm*, **15**, 6729-6735. http://dx.doi.org/10.1039/c3ce27007f

[19] Yu, W., Zhang, J. and Peng, T. (2016) New Insight into the Enhanced Photocatalytic Activity of N-, C- and S-Doped ZnO Photocatalysts. *Applied Catalysis B*: *Environmental*, **181**, 220-227. http://dx.doi.org/10.1016/j.apcatb.2015.07.031

[20] Rengaraj, S., Venkataraj, S., Tai, C., Kim, Y.H., Repo, E. and Sillanp, M. (2011) Self-Assembled Mesoporous Hierarchical-Like In_2S_3 Hollow Microspheres Composed of Nanofibers and Nanosheets and Their Photocatalytic Activity. *Langmuir*, **27**, 5534-5541. http://dx.doi.org/10.1021/la104780d

[21] Sajan, C.P., Wageh, S., Al-Ghamdi, A.A., Yu, J. and Cao, S. (2016) TiO_2 Nanosheets with Exposed {001} Facets for Photocatalytic Applications. *Nano Research*, **9**, 3-27. http://dx.doi.org/10.1007/s12274-015-0919-3

[22] Qi, K.Q., Wang, Y., Wang, R.D., Wu, D. and Li, G.D. (2016) Facile Synthesis of Homogeneous $CuInS_2$ Quantum Dots with Tunable Near-Infrared Emission. *Journal of Materials Chemistry C*, **4**, 1895-1899. http://dx.doi.org/10.1039/C5TC04232A

[23] Yu, W., Xu, D. and Peng, T. (2015) Enhanced Photocatalytic Activity of g-C_3N_4 for Selective CO_2 Reduction to CH_3OH via Facile Coupling of ZnO: A Direct Z-Scheme Mechanism. *Journal of Materials Chemistry A*, **3**, 19936-19947. http://dx.doi.org/10.1039/C5TA05503B

[24] Wetterskog, E., Tai, C.W., Grins, J., Bergström, L. and Salazar-Alvarez, G. (2013) Anomalous Magnetic Properties of Nanoparticles Arising from Defect Structures: Topotaxial Oxidation of $Fe_{1-x}O|Fe_{3-\delta}O_4$ Core|Shell Nanocubes to Single-Phase Particles. *ACS Nano*, **7**, 7132-7144. http://dx.doi.org/10.1021/nn402487q

[25] Low, J., Yu, J., Li, Q. and Cheng, B. (2014) Enhanced Visible-Light Photocatalytic Activity of Plasmonic Ag and Graphene Co-Modified Bi_2WO_6 Nanosheets. *Physical Chemistry Chemical Physics*, **16**, 1111-1120. http://dx.doi.org/10.1039/C3CP53820F

[26] Yang, Z.X., Zhang, P., Zhong, W., Deng, Y., Au, C.T. and Du, Y.W. (2012) Design, Growth, and Characterization of Morphology-Tunable $Cd_xZn_{1-x}S$ Nanostructures Generated by a One-Step Thermal Evaporation Process. *CrystEngComm*, **14**, 4298-4305. http://dx.doi.org/10.1039/c2ce25181g

[27] Li, Q., Meng, H., Zhou, P., Zheng, Y.Q., Wang, J., Yu, J.G. and Gong, J.R. (2013) $Zn_{1-x}Cd_xS$ Solid Solutions with Controlled Bandgap and Enhanced Visible-Light Photocatalytic H_2-Production Activity. *ACS Catalysis*, **3**, 882-889. http://dx.doi.org/10.1021/cs4000975

[28] Moon, G.D., Ko, S., Min, Y., Zeng, J., Xia, Y. and Jeong, U. (2011) Chemical Transformations of Nanostructured Materials. *Nano Today*, **6**, 186-203. http://dx.doi.org/10.1016/j.nantod.2011.02.006

[29] Li, W., Li, D., Zhang, W., Hu, Y., He, Y.H. and Fu, X. (2010) Microwave Synthesis of $Zn_xCd_{1-x}S$ Nanorods and Their Photocatalytic Activity under Visible Light. *The Journal of Physical Chemistry C*, **114**, 2154-2159. http://dx.doi.org/10.1021/jp9066247

[30] Han, D., Cao, J., Yang, S., Yang, J., Wang, B., Fan, L., Liu, Q., Wang, T. and Niu, H. (2014) Investigation of Composition Dependent Structural and Optical Properties of the $Zn_{1-x}Cd_xS$, Coaxial $Zn_{0.99-x}Cd_xCu_{0.01}S/ZnS$, $Zn_{0.99-x}Cd_xMn_{0.01}S$ Nanorods Generated by a One-Step Hydrothermal Process. *Dalton Transactions*, **43**, 11019-11026. http://dx.doi.org/10.1039/c4dt00667d

[31] Zhang, J., Shi, F., Chen, D., Gao, J., Huang, Z., Ding, X. and Tang, C. (2008) Self-Assembled

3-D Architectures of BiOBr as a Visible Light-Driven Photocatalyst. *Chemistry of Materials*, **20**, 2937-2941. http://dx.doi.org/10.1021/cm7031898

[32] Yang, F., Yan, N., Huang, S., Sun, Q., Zhang, L. and Yu, Y. (2012) Zn-Doped CdS Nanoarchitectures Prepared by Hydrothermal Synthesis: Mechanism for Enhanced Photocatalytic Activity and Stability under Visible Light. *The Journal of Physical Chemistry C*, **116**, 9078-9084. http://dx.doi.org/10.1021/jp300939q

[33] Hermann, J., Tahiri, H., Ait-Ichou, Y., Lassaletta, G., Gonzalez-Elipe, A. and Fernandez, A. (1997) Characterization and Photocatalytic Activity in Aqueous Medium of TiO_2 and Ag-TiO_2 Coatings on Quartz. *Applied Catalysis B: Environmental*, **13**, 219-228. http://dx.doi.org/10.1016/S0926-3373(96)00107-5

[34] Scalfani, A. and Hermann, J. (1998) Influence of Metallic Silver and of Platinum-Silver Bimetallic Deposits on the Photocatalytic Activity of Titania (Anatase and Rutile) in Organic and Aqueous Media. *Journal of Photochemistry and Photobiology A*, **113**, 181-188. http://dx.doi.org/10.1016/S1010-6030(97)00319-5

[35] Vamathevan, V., Amal, R., Beydoun, D., Low, G. and McEvoy, S. (2002) Photocatalytic Oxidation of Organics in Water Using Pure and Silver-Modified Titanium Dioxide Particles. *Journal of Photochemistry and Photobiology A*, **148**, 233-245. http://dx.doi.org/10.1016/S1010-6030(02)00049-7

[36] Li, X.Z. and Li, F.B. (2001) Study of Au/Au^{3+}-TiO_2 Photocatalysts toward Visible Photooxidation for Water and Wastewater Treatment. *Environmental Science & Technology*, **35**, 2381-2387. http://dx.doi.org/10.1021/es001752w